

# A Unified Framework for Automated Assembly Sequence and Production Line Planning using Graph-based Optimization

Christoph Hartmann<sup>a,1,\*</sup>, Marios Demetriades<sup>a,1</sup>, Kevin Prüfer<sup>a</sup>, Zichen Zhang<sup>a</sup>, Klaus Spindler<sup>b</sup>, Stefan Weltge<sup>c</sup>

<sup>a</sup>Technical University of Munich, Chair of Metal Forming and Casting, Walther-Meissner-Strasse 4, 85748 Garching, Germany

<sup>b</sup>Faurecia Emissions Control Technologies, Germany GmbH, Biberbachstrasse 9, 86154 Augsburg, Germany

<sup>c</sup>Technical University of Munich, Professorship for Discrete Mathematics, Boltzmannstrasse 3, 85748 Garching b. München, Germany

## Abstract

This paper presents PyCAALP (Python-based Computer-Aided Assembly Line Planning), a framework for automated Assembly Sequence Planning (ASP) and Production Line Planning (PLP), employing a graph-based approach to model components and joints within production modules. The framework integrates kinematic boundary conditions, such as potential part collisions, to guarantee the feasibility of automated assembly planning. The developed algorithm computes all feasible production sequences, integrating modules for detecting spatial relationships and formulating geometric constraints. The algorithm incorporates additional attributes, including handling feasibility, tolerance matching, and joint compatibility, to manage the high combinatorial complexity inherent in assembly sequence generation. Heuristics, such as Single-Piece Flow assembly and geometrical constraint enforcement, are utilized to further refine the solution space, facilitating more efficient planning for complex assemblies. The PLP stage is formulated as a Mixed-Integer Program (MIP), balancing the total times of a fixed number of manufacturing stations. While some complexity-reduction techniques may sacrifice optimality, they significantly reduce the MIP's computational time. Furthermore, the framework enables customization of engineering constraints and supports a flexible trade-off between ASP and PLP. The open-source nature of the framework, available at <https://github.com/TUM-utg/PyCAALP>, promotes further collaboration and adoption in both industrial and production research applications.

**Keywords:** Assembly Sequence Planning (ASP), Assembly Line Planning (ALP), Mixed-Integer Programming (MIP), Computer-Aided Process Planning (CAPP), Graph-based optimization

## 1. Introduction

Assembly Sequence Planning (ASP) and Production Line Planning (PLP) within factory planning are inherently complex, primarily due to the high-dimensional space in which they must be executed, encompassing product characteristics, production processes, and business requirements. Addressing these challenges, this paper introduces a concept for automating assembly and line planning, integrating key elements such as sequence planning, equipment selection, line configuration, and workforce allocation.

Product design has a critical influence on both assembly and disassembly operations. Consequently, frameworks like Design for Assembly (DfA) and Design for Disassembly (DfD) have become central to current research and industrial practice. As the manufacturing industry continues shifting toward customized products, the demand for automated and adaptable process planning solutions increases.

Despite the extensive data embedded within 3D models, the potential of these resources for enhancing manufacturing pro-

cess planning remains vastly underutilized. Leveraging this data from various 3D model formats could significantly optimize ASP and PLP, improving efficiency, adaptability, and overall effectiveness.

Another important aspect is accessibility. Python has become the standard language for various applications, due to its ease of use, free availability, and the variety of scientific libraries. We believe that this is the perfect combination for creating software that engineers can use, integrating with various industry workflows.

Taking these points into consideration, the proposed Python-based framework should tackle the challenges by integrating both ASP and PLP problems within a unified approach. It incorporates engineering, geometric, and manufacturing constraints to enhance realism and applicability. A Mixed-Integer Program (MIP)-based formulation is used under the assumption of a fixed number of workstations. The framework is designed to be data-efficient, user-friendly, and adaptable to real production environments. Additionally, it introduces a novel method for modeling geometric constraints by extracting individual degree-of-freedom matrices from a 3D model through joint analysis.

\*Abbreviations: ASP, Assembly Sequence Planning; PLP, Production Line Planning; DoF, Degree of Freedom; MIP, Mixed-Integer Program.

\*Corresponding author

Email address: [christoph.hartmann@utg.de](mailto:christoph.hartmann@utg.de) (Christoph Hartmann)

<sup>1</sup>These authors contributed equally to this work.

## 2. State of the art

Existing research on ASP and PLP focuses on developing computational methods that address their inherent complexity and provide efficient problem-solving algorithms.

### 2.1. Assembly planning

Various approaches have been developed to solve the ASP problem, i.e., determining the optimal assembly sequence given specific objectives or constraints. Most rely on a directed graph representation of the assembly, typically derived from a solid model. The graph nodes, representing components, may have a contact, blocking, or free relation with the other nodes in the graph. Early contributions utilized Degree of Freedom (DoF) matrices to enforce geometric constraints and capture the node relations for any pair of the assembly components and their surfaces. The matrix elements represent the available DoF in both positive and negative directions for translation and rotation. Furthermore, these contributions employed stability and accessibility constraints to secure parts and manage tool access restrictions [1]. The same constraints remain relevant in more recent methods. For instance, Lu et al [2] proposed a dynamic graph learning algorithm that integrates heuristic information into sequence optimization processes, improving performance and adaptability in complex assembly cases.

Other recent approaches have utilized deep learning methods for more complex assemblies (i.e., those comprising more than 1000 entities) to develop knowledge-enhanced graph embedding models [3], [4]. In addition, Shi et al. [5] applied named entity recognition to sequentially classify text data and output the type of various entities. Despite successfully embedding complex assemblies, these efforts do not directly solve an ASP problem. At the same time, many deep learning-based approaches require large, labeled datasets. Since these data are task-specific and company-dependent, their generalization is difficult. Thus, these methods are practically limited in highly customized environments.

Finally, multiple methods exist to find the optimal sequence, given an assembly graph. They include shortest path algorithms [6], greedy algorithms with feedback weights [7], and fitness-score based techniques on engineering constraints [2].

### 2.2. Line planning and time balancing

The PLP problem typically presents as an optimization problem that aims to distribute production process steps across various stages, while satisfying operational constraints. The most common approach is a MIP model, formulated based on constraints such as cycle time limits, precedence relations, and station capacities. The objective is to maximize the process output or the total cost for a given set of resources.

Beyond that, a wave of metaheuristic approaches complements the traditional exact methods. Genetic algorithms, simulated annealing, ant colony optimization, and particle swarm optimization have gained prominence due to their flexibility and effectiveness in handling complex and large-scale problems [8]. In addition, [9] implemented chance-constrained stochastic

models combined with a branch-and-bound and remember algorithm, which ensures solution feasibility under probabilistic constraints. Although not guaranteeing optimal solutions, most of these methods are simple, fast, robust, and often offer high-quality solutions, making them suitable for modern variable and complex manufacturing environments [10].

## 3. Problem Formulation

While significant advances have been made in both ASP and PLP, relatively few works attempt to integrate these aspects into a unified workflow. Our work aims to tackle this challenge and integrate both problems.

Formally, the problem transforms the physical assembly definition into a search space optimization defined by three components:

1. **Assembly Graph:** The part geometry is modeled as a connected undirected graph  $G_{part} = (N, J)$ , where  $N$  represents the set of components (nodes) and  $J$  represents the set of joints (edges).
2. **Weighted Directed Graph:** The solution space is mapped to a layered directed graph  $D = (V, E, W)$ . Here,  $V$  represents the assembly states (cutsets), and  $E$  the directed edges, corresponding to a joint operation between cutsets. The set of weights  $W$  assigns a weight  $w_e$  to each operation  $e \in E$ , derived from the engineering constraints.
3. **Objective Function:** The optimization goal is to minimize the global cost  $\mathcal{J}$ , defined as a weighted sum of the soft engineering constraints' cost ( $C_{eng}$ ) and the time balancing cost ( $C_{time}$ ). The two parts correspond to the ASP and the PLP, respectively:

$$\mathcal{J} = (1 - \lambda) \cdot C_{eng} + \lambda \cdot C_{time} \quad (1)$$

where  $\lambda \in [0, 1]$  is the user-defined influence factor controlling the trade-off between assembly sequence quality (engineering constraints) and assembly line efficiency (station time).

Therefore, given an input graph  $G_{part}$  and a fixed number of manufacturing stations, the objective is to find a path in  $D$  that minimizes  $\mathcal{J}$  subject to engineering and geometrical constraints. The engineering constraints (i.e., part fragility, manufacturing tolerances, and technological changes) are incorporated into the edge weights  $w_o$ , while the geometrical constraints define the feasible operations  $o$  when connecting a joint.

The assembly sequence and station time minimization problem of Eq. 1 is solved using an MIP, given the weighted directed graph  $D$  as input. In addition to the user-defined influence factor  $\lambda$ , the user can also control the relative weights of specific engineering constraints within  $w_o$ .

The ultimate goal is to find solutions fast and efficiently. For typical assemblies, ASP and PLP problems should be computed within minutes. For more complex assemblies, i.e., those consisting of more than 15 joints, the framework applies graph reduction techniques to reduce the size of  $D$ , producing a near-optimal solution within reasonable computational time.

## 4. Approach

Our approach tries to solve both ASP and PLP simultaneously. It consists of three steps: pre-processing, assembly planning, and line planning. Figure 1 illustrates the complete workflow, including functionalities and attributes/constraints per step. Ultimately, the best assembly path is calculated considering all constraints, with the option to prioritize either assembly or line planning.

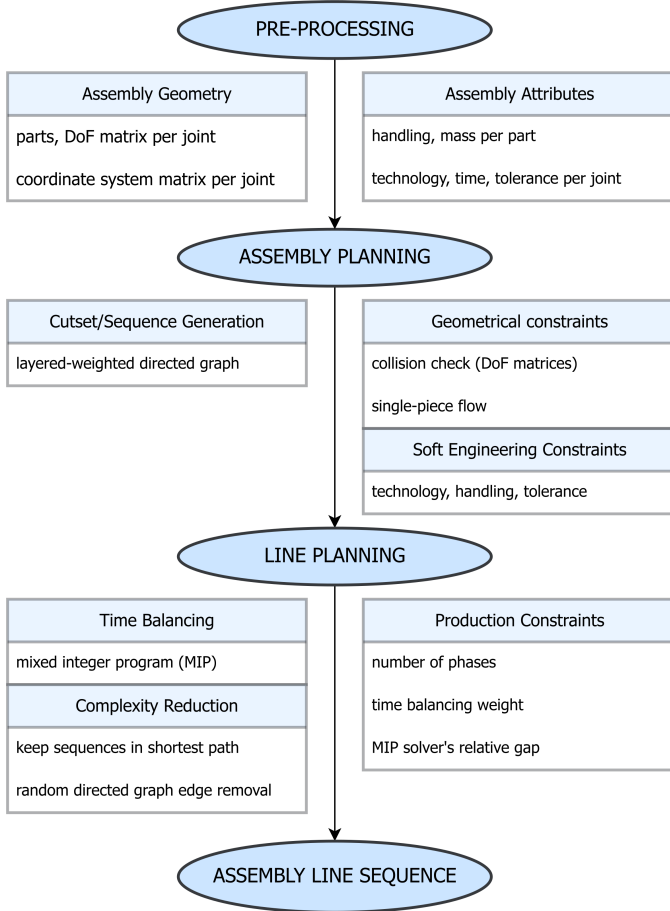


Figure 1: Workflow of the proposed unified framework. The process flows from CAD data pre-processing (extracting joints and DoF matrices) to Assembly Planning (generating the weighted directed graph with soft engineering and geometric constraints) and finally to Line Planning (solving the MIP for time balancing).

### 4.1. Pre-processing

In the first step, we utilize CAD models to automatically extract spatial information for use in the subsequent assembly planning step. Specifically, joints, DoF matrices, and coordinate systems are extracted for each joint. Furthermore, the assembly attributes (handling, mass per part, technology, time, and tolerance per joint) are assumed to be known.

### 4.2. Assembly planning

In the assembly planning step, all the possible assembly cutsets (an assembly connectivity state) and sequences are calculated while enforcing geometrical and engineering constraints.

The geometrical constraints are a combination of a heuristic and a collision check with DoF matrices. The user-defined technology, handling, and tolerance weights are used to construct a weighted directed graph, controlling the influence of these attributes. The output is a layered, weighted directed graph consisting of all the geometrically feasible sequences.

### 4.3. Line planning

In the final step, a time balancing problem, formulated as an MIP, solves the PLP. The user-defined production constraints determine the problem formulation, solution accuracy, and the influence of assembly and line planning in the solution. Furthermore, for complex cases, an optional operation utilizes a shortest path algorithm and a randomized edge removal to reduce the problem size. Finally, optimal assembly sequence and manufacturing stages planning can be extracted from the MIP's solution.

The user can run the workflow multiple times for various engineering and production constraints. In this case, the pre-processing stage should be executed only once. Thus, once the model data is available, only the assembly planning and time balancing stages need to be repeated.

## 5. Methods

This section provides a more in-depth coverage of the steps mentioned in Section 4 and illustrated in Fig 1. More precisely, the procedures, algorithms, and design of the Python-based framework are discussed.

### 5.1. Assembly part connection

In the first part of pre-processing, the assembly part connections are represented as an undirected graph, where nodes correspond to the assembly parts and edges correspond to the joints. The part information includes part names, weights, and handling instructions. Similarly, the joint information includes parts of the joint, time, and tolerance. Figures 4 and 3 show the graph representation of one of the two industrial assemblies (see Fig. 2) used for testing, along with the absolute values of the attributes, i.e., non-normalized, for joints or parts.

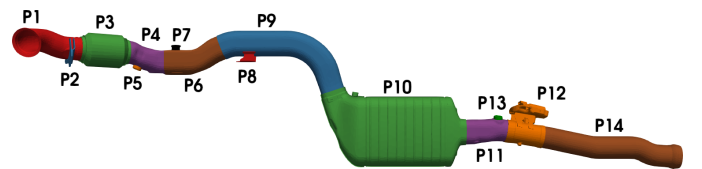
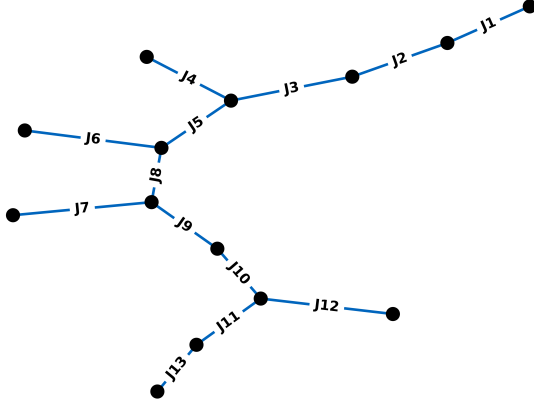


Figure 2: Assembly 1 geometry and part labels.

In practice, the part data are provided in a JSON file, and the graph is represented using NetworkX library [11]. All the attributes are then normalized to control the contribution to the overall weight of the next step's weighted directed graph.

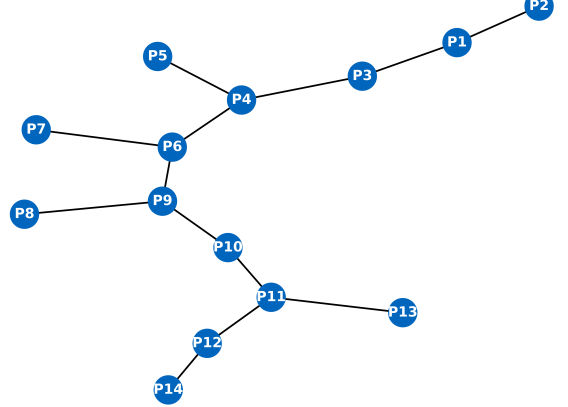
Assembly 1 joint attributes



	J1	J2	J3	J4	J5	J6	J7	J8	J9	J10	J11	J12	J13
<i>lw_len</i>	108	244.92	244.92	94.2	242	100.48	110	166	166	184.63	235.5	94.2	166
<i>tol</i>	10	6	8	4	6	7	4	7	3	8	4	8	3
<i>tech</i>	MAG2	MAG	MAG	MAG2	MAG	MAG	MAG2	MAG	MAG	MAG	MAG	MAG2	MAG

Figure 3: Graph representation of the joints (edges) for Assembly 1. Edge labels indicate the welding length [mm] (used as operation time in our model), tolerance value (integer 1-10, where higher values indicate stricter tolerances), and the joining technology type ("MAG" vs "MAG2")

Assembly 1 part attributes



	P1	P2	P3	P4	P5	P6	P7	P8	P9	P10	P11	P12	P13	P14
<i>mass</i>	1.112	0.138	1.917	0.731	0.03	1.081	0.052	0.129	2.45	6.831	0.768	1.473	0.03	2.29
<i>hand</i>	2	1	2	1	1	3	3	1	2	1	3	3	1	3

Figure 4: Graph representation of the parts (nodes) for Assembly 1. Node labels indicate component mass [kg] and the handling complexity level (normalized integer 1-3).

## 5.2. Degree of freedom matrices

The second part of the pre-processing deals with the DoF matrices. They are optionally extracted from the CAD files for use in the geometrical constraint enforcement, i.e., collision checking. This part consists of two operations: spatial relationship detection and geometrical constraint construction.

First, we export the CAD data into STL format, which employs a triangle mesh representation, by which the surfaces of the CAD models are stored as a set of triangle meshes.

The graphics libraries for the CAD part include PyVista (used for basic mesh operations), [12], Flexible Collision Library (FCL) [13], MeshLib [14], and trimesh [15].

### 5.2.1. Spatial relationship detection

To obtain a reasonable assembly sequence, the spatial relationships among the CAD models should be taken into account. There are three types of spatial relationships defined in this framework: contact relationships, blocking relationships, and free relationships. An appropriate data structure to store the spatial relationship information between each pair of CAD models is a graph. We denote this graph as a relational graph.

The three kinds of spatial relationships are defined as follows:

1. Two CAD models have a contact relationship if they physically interact.
2. Two CAD models have a blocking relationship if they do not have physical contact, but they will have collisions when translating one of them in some orientations.
3. Two CAD models have a free relationship if their relationship is neither contact nor blocking.

In practice, we implement the relational graph as a matrix. We denote this matrix as a relational matrix. Since the spatial

relationships are mutual, which means the spatial relationship between A and B is the same as that between B and A, the relational graph is undirected, and the relational matrix is symmetric.

Afterwards, we use FCL to detect contact relationships and PyVista to detect blocking relationships. FCL is employed to detect whether two given CAD models have collisions. The two CAD models will have a contact relationship if they have collisions. If the relationship is not a contact relationship, we use an approach based on the raytracing method from PyVista to detect whether the relationship is blocking. This approach will cast rays in predefined orientations starting from each vertex of one CAD model and detect whether these rays intersect with the other CAD model. If there is at least one ray from any of the vertices that intersects with the other CAD model, the two CAD models will have a blocking relationship.

### 5.2.2. Geometric constraint construction

Furthermore, additional geometric constraints are crucial to ensure that the assembly sequence is reasonable. These geometric constraints are in the format of a DoF matrix, which gives more detailed spatial information among the CAD models.

A DoF matrix, as in Eq. (2), is a three-by-four matrix containing twelve elements representing the corresponding translational and rotational DoF.  $T$  and  $R$  are translational DoF and rotational DoF matrices, respectively. There are actually three translational DoF and three rotational DoF in a 3D space. In this framework, we split each DoF into two, based on orientations. For instance, the translational DoF matrix in x orientation is split into one translational DoF in positive x orientation and one translational DoF in negative x orientation.

$$M = \begin{pmatrix} T_{+x} & T_{-x} & R_{+x} & R_{-x} \\ T_{+y} & T_{-y} & R_{+y} & R_{-y} \\ T_{+z} & T_{-z} & R_{+z} & R_{-z} \end{pmatrix} \quad (2)$$

Note that these DoF matrices are only constructed for CAD model pairs with a contact or blocking relationship. To obtain these DoF, corresponding geometric movements are applied to a CAD model from a given pair, and the intersection volume between the moved CAD model and the other CAD model from this pair is computed using MeshLib. If the volume is not zero, the corresponding DoF for the moved CAD model will be zero. For example, we apply a geometric translational movement in the positive x orientation to a CAD model. If the intersection volume between it and the other CAD model is not zero, then the translational DoF in the positive x orientation for the moved CAD model is zero. To ensure a more robust detection, a set of translational distances and a set of rotational angles are pre-defined for multiple detections. A small example of DoF matrix extraction is shown in Appendix A.

Furthermore, the DoF matrices and a unique coordinate system per joint are provided in JSON format to serve as geometrical constraints during the assembly planning process.

### 5.3. Cutset/sequence generation

After gathering all important assembly information, the generation of the cutset/sequence layered digraph follows. In this step, the cutsets are represented by weighted directed graph nodes, where the number of layers equals the number of assembly joints + 1, i.e., one joint addition per layer. Each edge corresponds to a joint addition, and each node to a unique cutset state. A cutset state corresponds to a distinct structural connectivity of the partially assembled product. The weights of the graph's edges are calculated using the user-defined weighted constants ( $\mu$ ) for technology, handling, and tolerance (see Eq. 3). These constants give control over the assembly planning.

Let  $\mu_{tech}, \mu_{hand}, \mu_{tol} \in [0, 1]$  be the user-defined weights such that  $\mu_{tech} + \mu_{hand} + \mu_{tol} = 1$  and  $l_e \in [1, L]$  be the directed graph's layer of edge  $e$ . The calculation for the weight  $w_e$  of an edge  $e$ , assuming that all attribute weights are normalized, is given by:

$$w_e = \frac{\mu_{tech} \cdot w_{tech}(e) + \mu_{hand} \cdot w_{hand}(e) + \mu_{tol} \cdot w_{tol}(e)}{l} \quad (3)$$

The directed graph is generated using a two-step fused method. Initially, using the connected assembly graph, all the possible cutsets are obtained by removing one edge at a time. For each step, i.e., edge removal, one layer is created in the directed graph, and all of its nodes consist of assembly graphs with an equal number of edges. The final node of the directed graph is the disconnected assembly graph. Thus, the directed graph is generated starting from its last layer, the fully connected part.

Equation 4 shows the maximum possible number of edges  $|E|$  of the directed graph, for a given number of assembly joints ( $J$ ). The solution space of a directed graph created by a relatively big assembly increases dramatically. For example, a directed graph representing an assembly with 17 joints might have more than 1.2 million edges. A slightly more complex assembly, consisting of 20 joints, might have ten million edges. Trying to solve the MIP of the PLP stage may result in an unreasonable solving time. Therefore, geometrical constraining methods are

utilized to decrease the solution space. Engineering constraints or heuristics are applied when creating new edges in the directed graph. First, with the removal of an edge, the resulting assembly graph should consist of a single subassembly, meaning that the actual manufacturing process operates with only one assembly, thereby enforcing Single-Piece Flow.

$$|E|_{max} = \sum_{j=0}^{J-1} (J-j) \binom{J}{j} \quad (4)$$

### 5.4. Collision check

In addition, using the DoF matrices, a collision scenario is checked, excluding infeasible edge removals and enforcing the geometrical constraints. First, this check is optional and available only for assemblies with generated DoF matrices. We use this functionality later for assembly 2. For the other assemblies, this step is skipped.

The check is a multi-step process with the following order:

1. For every new joint added to a cutset, find connected edges of the new part.
2. Check if the other part of the joint (not the new part) is connected to the current graph/cutset.
3. Transform the DoF matrices to the reference coordinates, i.e., the ones of the new edge. Notice that each edge has its own coordinate system matrix.
4. Make collision check, i.e., compare available translational movements.
5. If there are available translational movements, then the new edge may be created in the directed graph.

Finally, all the edges in the cutset-directed graph have a calculated single weight, which will be used in the next steps for an optional directed graph complexity reduction and for the MIP.

A complete algorithm is presented in Appendix B, detailing all the steps required to create the assembly-weighted directed graph.

### 5.5. Cutset complexity reduction

In the previous step, the geometrical constraints reduced the size of the directed graph. Nevertheless, for relatively larger assemblies, i.e., those with more than 20 components, the directed graph's solution space still renders the next step's MIP unsolvable within a reasonable time. Thus, in this optional stage, the cutset complexity, i.e., the number of directed graph's edges, is reduced. Initially, multiple shortest paths are calculated. The goal is to preserve the nodes of various shortest paths, calculated based on the edge weight values. Then, an edge filtering procedure randomly removes a percentage of each layer's edges, while protecting the ones that appeared in the previous shortest path calculation. Some outer layers of the assembly digraph are protected to avoid eliminating initial and final nodes. The result is a reduced weighted directed graph providing a smaller solution space for the PLP problem.

### 5.6. Time balancing

The final part of the procedure addresses the PLP problem for a given number of manufacturing stations. This problem is tackled with the use of a MIP and the cost function in ef. 1. The formulated MIP's objective function is presented in Eq. (5) and the constraints from Eq. (6) to (14). The current problem attempts to assign each operation, i.e., joint, to the correct phase, i.e., manufacturing station, considering the assembly directed graph's edge weights and the maximum phase time.

$$\min (1 - \lambda) \sum_{e \in E} (w_e x_e) + \lambda c \alpha \quad (5)$$

$$\text{s.t.} \quad \sum_{e \in \text{out\_edges}(v_{\text{start}})} x_e = 1 \quad (6)$$

$$\sum_{e \in \text{in\_edges}(v_{\text{end}})} x_e = 1 \quad (7)$$

$$\sum_{e \in \text{in\_edges}(v)} x_e = \sum_{e \in \text{out\_edges}(v)} x_e \quad \forall v \in V \setminus \{v_{\text{start}}, v_{\text{end}}\} \quad (8)$$

$$\sum_{p=0}^{P-1} y_{l,p} = 1 \quad \forall l \in \{0, \dots, L-1\} \quad (9)$$

$$y_{l,0} \leq y_{l-1,0} \quad \forall l \in \{1, \dots, L-1\} \quad (10)$$

$$y_{l,p} \leq y_{l-1,p-1} + y_{l-1,p} \quad \forall l, p \in \{1, \dots, P-1\} \quad (11)$$

$$\sum_{p=0}^{P-1} z_{o,p} = 1 \quad \forall o \in O \quad (12)$$

$$z_{o(e),p} \geq x_e + y_{l(e),p} - 1 \quad \forall e \in E, p \in \{0, \dots, P-1\} \quad (13)$$

$$\alpha \geq \sum_{o \in O} z_{o,p} \cdot t_o \quad \forall p \in \{0, \dots, P-1\} \quad (14)$$

We define the notation as follows:  $w_e$  is the assembly-directed graph weight of edge  $e$ .  $c$  is an equal contribution factor that is pre-calculated to enforce equal contribution of assembly and line planning parts, i.e., in the objective value.  $\lambda \in [0, 1]$  is a user-defined time-balancing coefficient which controls the contribution of ASP and PLP.  $E$  is the set of edges in the directed graph.  $V$  is the set of nodes (cutsets) in the directed graph.  $O$  is the set of physical operations (joints).  $P$  is the number of phases (stations).  $L$  is the number of layers.  $l(e)$  denotes the layer index to which edge  $e$  belongs.  $o(e)$  denotes the operation corresponding to edge  $e$ .  $t_o$  is the operation time required for operation  $o$ .  $x_e \in \{0, 1\}$  indicates whether edge  $e$  is used.  $y_{l,p} \in \{0, 1\}$  assigns directed graph's layer  $l$  to phase  $p$ .  $z_{o,p} \in \{0, 1\}$  assigns operation  $o$  to phase  $p$ .  $\alpha$  denotes the maximum time of any phase.

The constraints can be described as follows: The first three constraints deal with the  $x$  variable. Equation (6) requires the sum of all outgoing edges of the start node  $v_{\text{start}}$  to be one. Similarly, Eq. (7) enforces the sum of all ingoing edges of the end node  $v_{\text{end}}$  to be one. Equation (8) ensures the flow conservation for all the other nodes, i.e., the sum of ingoing and outgoing edges is equal. The next three constraints deal with the  $y$  variable. Equation (9) ensures that each layer has only one phase assigned. Equations (10) and (11) impose the monotonicity constraint for all the phases, ensuring that the phases are assigned to layers in ascending order. Equation (12) ensures that each operation is assigned precisely one phase. The three binary variables,  $x, y, z$ , are linked with Eq. (13). The fi-

nal constraint (Eq. (14)) ensures that the  $\alpha$  continuous variable calculates the maximum load of a phase.

The optimal sequence and operations per phase are taken from the  $x$  and  $z$  binary variables. From the solution of the MIP problem, many valuable results can be extracted. First, the joint sequence and the attributes of the joint and parts for each operation. This could be used to check the attribute changes (technology) or development (handling, tolerance). Additionally, the phase/station times are the values we aim to minimize for the PLP problem.

We utilized the PySCIPOpt library [16] to solve the problem computationally.

## 6. Results

After implementing the computational framework, we evaluated its correctness and performance. The computational experiments were conducted on two industrial assemblies.

### 6.1. Experimental Setup

The first industrial assembly (Assembly 1) consists of 14 parts and 13 joints (Figs. 3, 4). This assembly serves as the baseline for verifying the correctness of the framework. We used Assembly 1 to analyze the sensitivity of the objective function to the user-defined engineering weights ( $\mu$ ) and the time-balancing factor ( $\lambda$ ).

The second assembly (Assembly 2) consists of 15 parts and 17 joints (see Appendix C). According to Eq. (4), the upper bound for the directed graph edges is 1,245,167 ( $\approx 1.2 \times 10^6$ ), compared to Assembly 1, 61,427 ( $\approx 6.1 \times 10^4$ ), increasing the complexity of the problem by nearly two orders of magnitude. Therefore, Assembly 2 provides a suitable test case to evaluate the effectiveness of the geometrical constraints, i.e., DoF matrices, the directed graph edge reduction method, and the increase in the solution's relative gap, in maintaining optimal solutions for high-complexity scenarios.

The experiments were conducted on local workstations equipped with an Intel Core i5-14500 CPU (2.60 GHz) and 32 GB of RAM.

### 6.2. Validation for optimization objectives

This section utilizes Assembly 1 to verify that the proposed objective function  $\mathcal{J}$  correctly solves the ASP and PLP problems according to user-defined priorities. We assess the solver's responsiveness to specific manufacturing constraints by varying the engineering weights ( $\mu$ ) and the time-balancing factor ( $\lambda$ ). For all validation tests, the number of phases was fixed at  $P = 3$ .

#### 6.2.1. Sensitivity to engineering weights ( $\mu$ )

We analyzed the impact of technology, handling, and tolerance weights on the optimal assembly structure. In each scenario, one engineering constant was prioritized (set to 1.0), while the other two were ignored (set to 0.0).

Assembly 1 consists of two different technologies ("MAG" and "MAG2"), as shown in Figure 3. In that case, the minimum

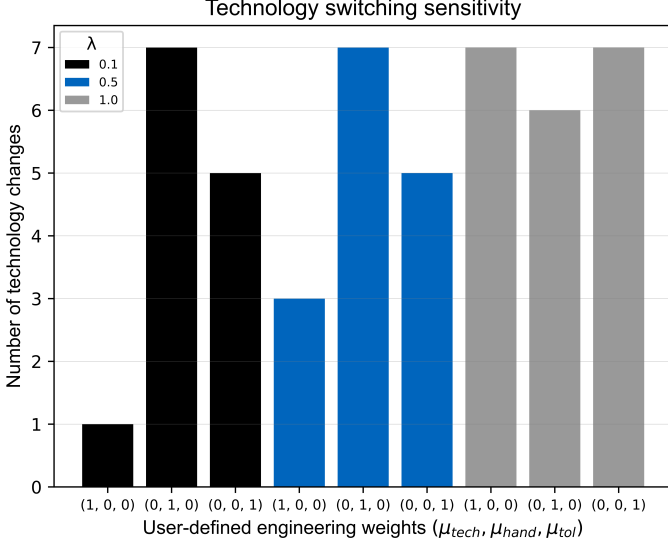


Figure 5: Impact of engineering weights ( $\mu$ ) on technology changes. When ASP and  $\mu_{tech}$  are prioritized, the solver identifies the theoretical minimum of 1 change. On other occasions, there are up to 8 random changes.

possible number of technology changes is one, i.e., switching from one manufacturing technology to the other. In addition, three time balancing weight values were used ( $\lambda = 0.1, 0.5, 1.0$ ). Figure 5 shows the number of technology changes presented in the optimal assembly sequence. The results show that when the technology weight is prioritized ( $\mu_{tech} = 1.0$ ), and the time-balancing influence is low to moderate ( $\lambda < 0.5$ ), the solver attempts to minimize the number of technology changes. In the case of  $\lambda = 0.1$ , the minimum possible technology change of one is achieved. In contrast, the other scenarios with no technology prioritization ( $\mu_{tech} = 1.0$ ) and/or a higher time-balancing factor ( $\lambda = 1.0$ ) resulted in up to eight technology changes. Therefore, the solver correctly penalizes technology switching when  $\mu_{tech}$  is prioritized.

In the next step, we evaluated the handling and tolerance constraints. The optimization objective is to minimize the cumulative value of these attributes by prioritizing sequences with lower part fragility and relaxed tolerance requirements. We fixed the time-balancing factor at  $\lambda = 0.5$  to ensure an equal trade-off between the soft engineering constraints and time balancing. Figures 6 and 7 show the cumulative development of the attribute costs over the assembly sequence steps. In both cases, when the attribute in focus was prioritized ( $\mu_{hand} = 1$  or  $\mu_{tol} = 1$ ), the accumulation curve is notably shallower compared to the other runs. The smaller area under these curves confirms that the objective function effectively minimizes the specific cumulative cost of the chosen attribute.

### 6.2.2. Sensitivity to time-balancing factor ( $\lambda$ )

Finally, we evaluated the influence of the time-balancing factor ( $\lambda$ ) on production line efficiency. By definition, increasing  $\lambda$  prioritizes the time-balancing problem over the PLP problem, aiming to minimize the maximum phase time ( $\alpha$ ). We use the assembly welding length as an indirect representation of time.

Figure 8 illustrates the maximum phase welding length

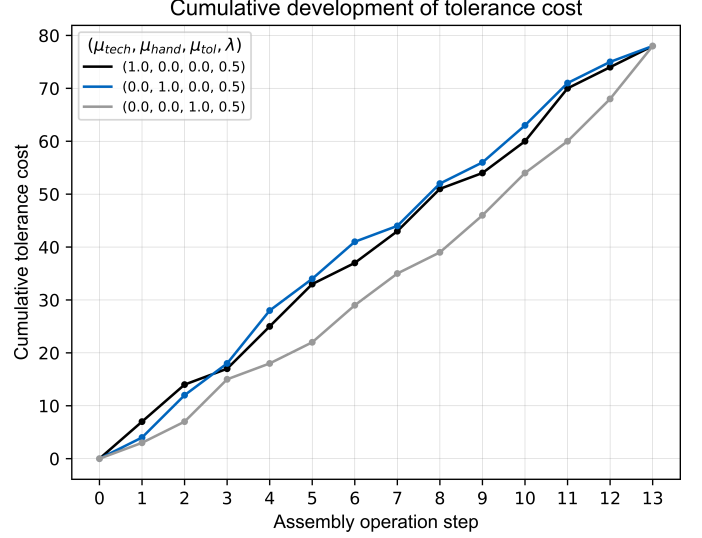


Figure 6: Cumulative development of absolute tolerance costs over the assembly sequence. Prioritizing tolerance ( $\mu_{tol} = 1.0$ , gray line) results in a shallower accumulation curve compared to non-prioritized runs. Note that tolerance is modeled as a normalized cost, where higher values indicate stricter tolerances.

across varying  $\lambda$  values. The data shows a downward trend in phase welding length as  $\lambda$  approaches 1.0. Thus, the parameter  $\lambda$  serves as a mechanism for regulating the trade-off between phase time and sequence optimality.

### 6.3. Computational efficiency and scalability

This section evaluates the framework's performance on the complex Assembly 2, focusing on the impact of physical constraints, i.e., collision checks, and the randomized edge reduction methods on the computational time and solution quality.

#### 6.3.1. Geometrical constraints effect

For this assembly, the solution space is significantly larger, with a theoretically maximum of approximately  $1.2 \times 10^6$  edges. However, enabling the collision check using DoF matrices during directed graph creation reduced the number of edges by 45% compared to a run without enforcing geometrical constraints. This DoF reduction step significantly decreases the graph size before the PLP phase begins, and it is essential for handling complex assemblies.

#### 6.3.2. Randomized edge reduction

To further reduce the solving time, we applied the randomized edge reduction method, varying from 0% to 70% in increments of 10%. The aim is to assess the balance between the computational efficiency (speedup) and solution quality. The MIP solver's relative gap was set to 0%. As with the previous test, the number of phases is kept at  $P = 3$ .

**Speedup:** Figure 9 shows the speedup, defined as the total MIP execution time with 0% reduction divided by the respective time of a reduced time case. The dashed line indicates the speedup value of 1, i.e., the baseline for the decrease in runtime. The results show a significant decrease in runtime, especially for a reduction of 70%, reaching a speedup of approximately



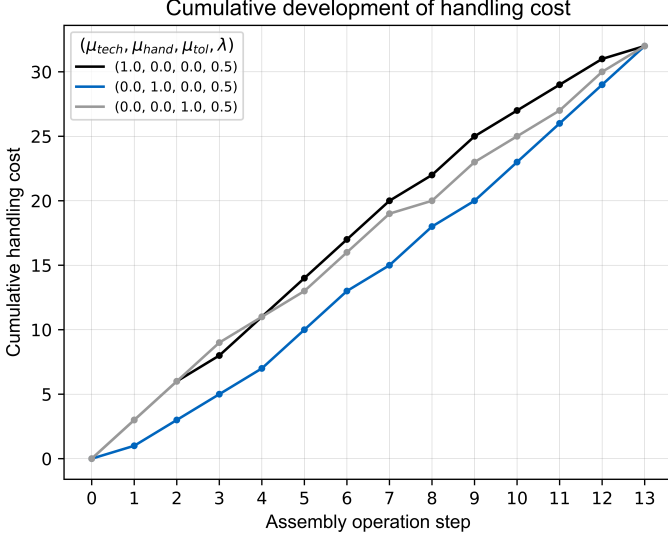


Figure 7: Cumulative development of handling costs. Prioritizing the handling attribute ( $\mu_{hand} = 1.0$ , blue line) minimizes the total handling complexity of the sequence. Note that handling is modeled as a normalized cost, where higher values indicate higher fragility.

550 $\times$ . The reduction from hours ( $t_{0\%} \approx 6.7hrs$ ) to minutes ( $t_{70\%} = 44sec$ ) confirms that the framework can generate solutions quickly enough for industrial applications.

**Solution quality:** Figure 10 (black line) illustrates the effect of the random edge reduction method on the maximum phase time. The maximum phase time remains unchanged for reductions up to 60%. Even at 70% reduction, the increase is limited to 0.11%, which is negligible. Consequently, the substantial computational speedup obtained for the last reduction case outweighs the marginal loss in solution quality.

### 6.3.3. Relative gap effect

Another aspect we investigated is the influence of MIP’s relative gap on the resulting solution quality. Increasing the relative gap might result in reduced computation time while maintaining the solution space unchanged or slightly reduced. For this text, we set the relative gap to 3% and repeated the randomized edge reduction experiment on Assembly 2. Under this setting, the MIP runtime without edge reduction is  $t_{0\%} = 0.49hr$  compared to  $t_{0\%} \approx 6.7hr$  for a relative gap of 0%. This corresponds to a speedup factor of 13.7 for the zero-graph pruning case.

However, the maximum phase time across the experiment increased by up to 2.44%, (922 mm compared to 900 mm for the minimum value for the previous experiment - black line), which may be non-negligible in certain production settings (see Fig. 10 - blue line).

For practical purposes, we recommend applying the edge reduction strategy with a reduction of approximately 60 – 70%, which provides a favorable balance between near-optimal solution quality and significant computational speedup.

## 7. Conclusions

This work presented a unified, open-source computational framework for automated ASP and PLP. By integrating graph-

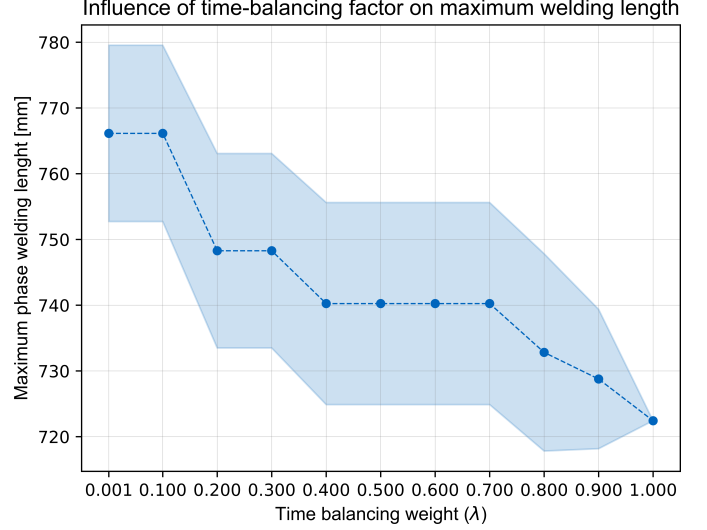


Figure 8: Influence of the time-balancing factor  $\lambda$  on the maximum phase welding length, indirectly on the phase time  $\alpha$ . The shaded region represents  $\pm 1$  standard deviation. As  $\lambda \rightarrow 1$ , the system effectively prioritizes cycle time minimization.

based modeling with MIP optimization, the framework successfully bridges the gap between product design parameters and production line efficiency.

Experimental validation on industrial assemblies demonstrated the framework’s capabilities to handle complex combinatorial cases. The integration of geometric constraints, i.e., the DoF matrix-based collision detection, proved effective by pruning approximately 45% of infeasible operations before the MIP optimization step. Furthermore, the proposed randomized edge reduction algorithm, which incorporates protection of several cutsets included in various shortest paths, addresses the scalability challenge of PLP. Results showed that for complex assemblies, the framework achieves a computational speedup of 550 $\times$  while maintaining a solution quality within 0.11% of the baseline. In comparison, although relaxing the MIP relative gap also reduces the computation time, it introduces a more noticeable degradation in solution quality, making the proposed edge-reduction strategy the more reliable choice.

Additionally, the sensitivity analysis confirmed that the unified objective function  $\mathcal{J}$ , with the use of the parameters  $\lambda$  and  $\mu$ , effectively controls the trade-off between ASP’s (technology change, fragility, tolerance accumulation) and PLP’s qualities (manufacturing station time).

Future research will focus on incorporating more engineering and time balancing constraints, such as total cost and component mass, to address the full range of requirements of a manufacturing scenario. Additionally, integrating automatic data extraction from the CAD models will help to eliminate the need for manual input. Finally, the open-source nature of this framework encourages further collaboration and adoption in both industrial and research settings within the manufacturing domain.



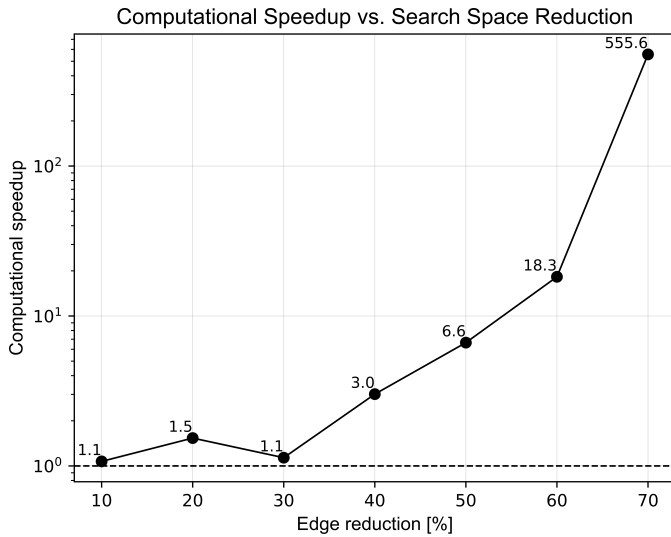


Figure 9: Computational speedup for Assembly 2. At edge reduction of 70%, the framework achieves a speedup factor of 550× compared to the baseline.

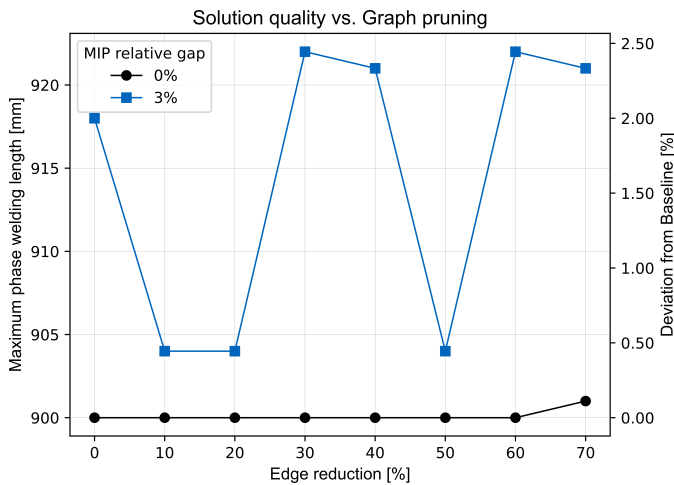


Figure 10: Impact of edge reduction on solution quality for Assembly 2 for 2 different relative gap settings.

## Acknowledgements

The authors would like to thank the Bavarian State Ministry of Economic Affairs, Regional Development and Energy (StMWi) for funding this project (number DIK0280/04).

## References

1. Laperrière L, Elmaraghy H. Gapp: A generative assembly process planner. *Journal of Manufacturing Systems* 1996;15:282–93. URL: <https://api.semanticscholar.org/CorpusID:109708282>.
2. Xia L, Lu J, Lu Y, Gao W, Fan Y, Xu Y, Zhang H. Semantic knowledge-driven a-gaseq: A dynamic graph learning approach for assembly sequence optimization. *Computers in Industry* 2024;154:104040. URL: <https://www.sciencedirect.com/science/article/pii/S0166361523001902>.
3. Jing Y, Zhou G, Zhang C, Chang F, Yan H, Xiao Z. Xmk: Explainable manufacturing knowledge recommendation for collaborative design with graph embedding learning. *Advanced Engineering Informatics* 2024;59:102339. URL: <https://www.sciencedirect.com/science/article/pii/S1474034623004676>.
4. Shi X, Tian X, Gu J, Yang F, Ma L, Chen Y, Su T. Knowledge graph-based assembly resource knowledge reuse towards complex product assembly process. *Sustainability* 2022;14(23). URL: <https://www.mdpi.com/2071-1050/14/23/15541>.
5. Shi X, Tian X, Ma L, Wu X, Gu J. A knowledge graph-based structured representation of assembly process planning combined with deep learning. *The International Journal of Advanced Manufacturing Technology* 2024;133(3–4):1807–1821. URL: <https://link.springer.com/article/10.1007/s00170-024-13785-4>.
6. Laperrière L, ElMaraghy HA. Assembly sequences planning for simultaneous engineering applications. *The International Journal of Advanced Manufacturing Technology* 1994;9(4):231–244. URL: <https://link.springer.com/article/10.1007/BF01751121>.
7. Zhu X, Xu Z, Wang J, Yang X, Fan L. Graph-based assembly sequence planning algorithm with feedback weights. *The International Journal of Advanced Manufacturing Technology* 2023;125(7–8):3607–3617. URL: <https://link.springer.com/article/10.1007/s00170-022-10639-9>.
8. Boysen N, Schulze P, Scholl A. Assembly line balancing: What happened in the last fifteen years? *European Journal of Operational Research* 2022;301(3):797–814. URL: <https://www.sciencedirect.com/science/article/pii/S0377221721009942>.
9. Li Z, Sikora CGS, Kucukkoc I. Chance-constrained stochastic assembly line balancing with branch, bound and remember algorithm. *Annals of Operations Research* 2024;335:491–516. URL: <https://doi.org/10.1007/s10479-023-05809-1>.
10. Ahmad AH, Azmir OS, Osman SA, Azhar MFAM, Jamaludin MH, Bakar HAA, Rahman MIA, Kiat TS. A

comprehensive review: Analysing the pros and cons of assembly line balancing methods. *Journal of Advanced Research in Applied Sciences and Engineering Technology* 2024;44(2):72–88. doi:10.37934/araset.44.2.7288.

11. Hagberg AA, Schult DA, Swart PJ. Exploring network structure, dynamics, and function using networkx. In: Varoquaux G, Vaught T, Millman J, eds. *Proceedings of the 7th Python in Science Conference*. Pasadena, CA USA; 2008:11–5. Version. 3.4.2.
12. Sullivan B, Kaszynski A. PyVista: 3D plotting and mesh analysis through a streamlined interface for the Visualization Toolkit (VTK). *Journal of Open Source Software* 2019;4(37):1450. URL: <https://doi.org/10.21105/joss.01450>. doi:10.21105/joss.01450; version. 0.45.2.
13. Automation B. python-fcl: Python bindings for the flexible collision library (fcl). <https://github.com/BerkeleyAutomation/python-fcl>; 2023. Version. 0.7.0.8.
14. MeshInspector . Meshlib: An sdk to supercharge your 3d data processing efficiency. <https://pypi.org/project/meshlib>; 2025. Version. 3.0.6.229.
15. Dawson-Haggerty M, et al. Trimesh: A python library for loading and using triangular meshes with an emphasis on watertight surfaces. <https://trimesh.org/>; 2022. Version 4.6.13.
16. Maher S, Miltenberger M, Pedroso JP, Rehfeldt D, Schwarz R, Serrano F. PySCIOpt: Mathematical programming in python with the SCIP optimization suite. In: *Mathematical Software – ICMS 2016*. Springer International Publishing; 2016:301–7. doi:10.1007/978-3-319-42432-3\_37; version 5.0.1.

## Appendix A. DFM extraction case study

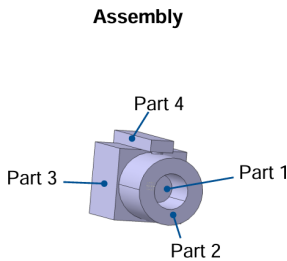


Figure A1: The assembly for the case study.

To clearly illustrate the DoF extraction method described in Section 5, we constructed an assembly comprising four parts, as shown in Figure A1. We used this assembly to show our approach in detail. We first export these CAD models into STL format. Then, spatial relationship detection is applied to build the relational matrix. We denote the contact, blocking, and free

relationships as 1, 2, and 3, respectively. The relationship between one part and itself is denoted as zero. The relational matrix  $RM$  is as (A.1).

$$RM = \begin{pmatrix} 0 & 2 & 1 & 1 \\ 2 & 0 & 1 & 1 \\ 1 & 1 & 0 & 1 \\ 1 & 1 & 1 & 0 \end{pmatrix} \quad (\text{A.1})$$

We define relevant joint coordinates for the next step and perform geometric constraint construction. For instance, the DoF matrix of part 1 with joint 13 under coordinate system 1 is as (A.2).

$$DoFM = \begin{pmatrix} 1 & 1 & 0 & 0 \\ 1 & 1 & 0 & 0 \\ 1 & 0 & 1 & 1 \end{pmatrix} \quad (\text{A.2})$$

## Appendix B. Assembly planning directed graph algorithm

This appendix outlines the algorithm used to generate the weighted directed graph  $D(V, E, W)$ , given a part graph  $G(N, J)$ . The algorithm iteratively explores the solution space by simulating the disassembly process (removing joints from the part graph) to generate layers in the directed graph. It strictly enforces the Single-Piece Flow constraint and utilizes DoF matrices to check for collisions during joining and prune geometrically infeasible sequences.

### Algorithm 1 Assembly weighted directed graph generation

---

**Require:** Assembly Graph  $G_{part} = (N, J)$ , DoF, Weights  $\mu$   
**Ensure:** Weighted Directed Graph  $D = (V, E, W)$

```

1:  $V_{layers} \leftarrow \{\}$  ▷ Stores valid cutsets per layer
2:  $D \leftarrow$  empty directed graph
3:  $L \leftarrow |J|$  ▷ Total number of layers
4:  $G_{sub} \leftarrow G_{part}$ 
5: for  $k \leftarrow 0 : L - 1$  do ▷ Iterate through layers
6:    $V_{layers}[k + 1] \leftarrow \{\}$ 
7:   for all subsets  $J_{rem} \subseteq J$  where  $|J_{rem}| = k + 1$  do
8:      $G_{sub} \leftarrow \text{remove\_edges}(G_{part}, J_{rem})$ 
9:     if IsConnected( $G_{sub}$ ) then ▷ Single-Piece Flow Constraint
10:       $V_{layers}[k + 1] \leftarrow V_{layers}[k + 1] \cup \{G_{sub}.edges()\}$ 
11:      for all  $E_{prev} \in V_{layers}[k]$  do
12:        if is_subset( $G_{sub}.edges, E_{prev}$ ) then
13:          if CollisionFree( $G_{sub}, DoF$ ) then ▷ DoF check
14:             $e \leftarrow \text{create\_transition}(E_{prev}, G_{sub})$ 
15:             $w_e \leftarrow \text{Eq. (3)}$  ▷ Calculate  $\mu$ -weighted cost
16:             $D.add\_edge(e, w_e)$ 
17:          end if
18:        end if
19:      end for
20:    end if
21:     $G_{sub} \leftarrow \text{restore\_edges}(G_{part}, J_{rem})$ 
22:  end for
23:   $\text{prune\_dead\_ends}(V_{layers}[k + 1])$  ▷ Remove nodes without successors
24: end for
25: return  $D$ 
```

---

## Appendix C. Dataset specification for Assembly 2

This appendix presents Assembly 2, comprising 17 joints (Fig. C2) and 15 parts (Fig. C3). It serves as the high-

complexity benchmark for the scalability experiment presented in Subsection 6.3.

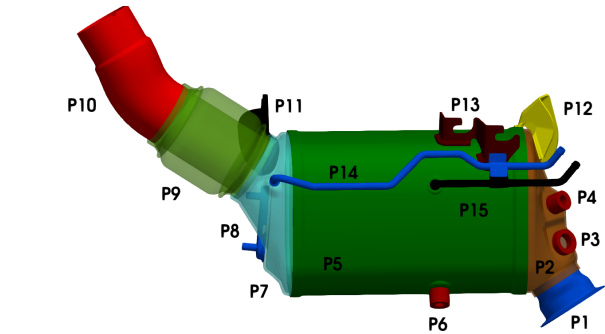


Figure C1: Assembly 2 geometry and part labels.

### Assembly 2 part attributes

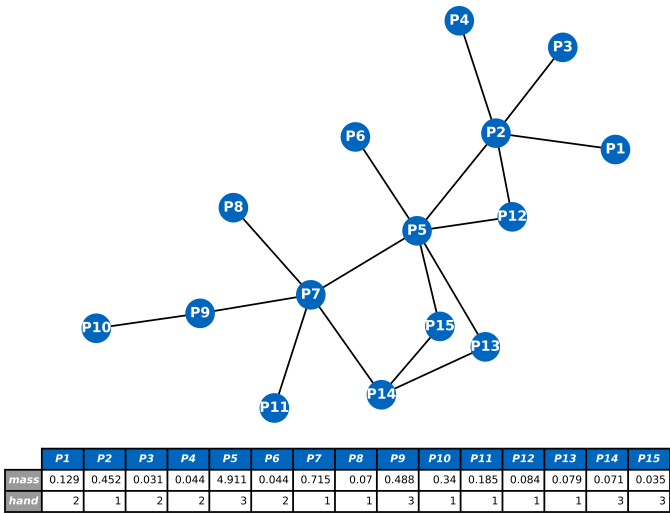


Figure C3: Graph representation of the components (nodes) for Assembly 2. Node labels indicate component mass [kg] and the handling complexity level (integer 1-3, where higher values indicate higher fragility).

### Assembly 2 joint attributes

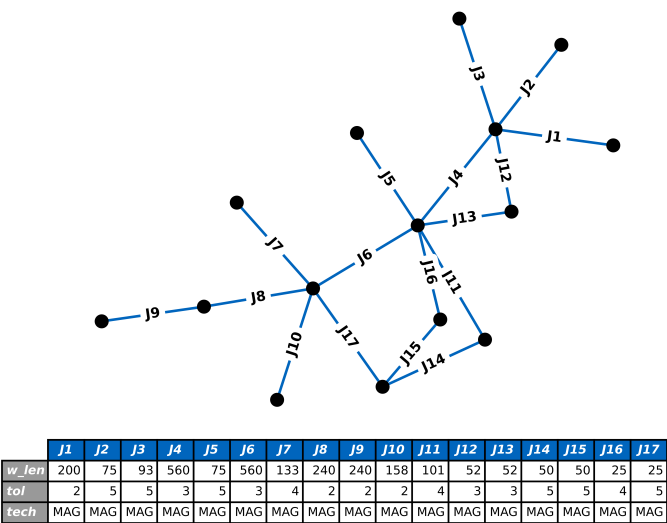


Figure C2: Graph representation of the connections (edges) for Assembly 2. Edge labels indicate the welding length [mm] (used as operation time in our model), tolerance value (integer 1-5, where higher values indicate stricter tolerances), and the joining technology type (only "MAG").